

# Comprehensive comparison of pore-scale models for multiphase flow in porous media

**Citation for published version:**

Zhao, B, MacMinn, CW, Primkulov, BK, Chen, Y, Valocchi, AJ, Zhao, J, Kang, Q, Bruning, K, McClure, JE, Miller, CT, Fakhari, A, Bolster, D, Hiller, T, Brinkmann, M, Cueto-Felgueroso, L, Cogswell, DA, Verma, R, Prodanović, M, Maes, J, Geiger, S, Vassvik, M, Hansen, A, Segre, E, Holtzman, R, Yang, Z, Yuan, C, Chareyre, B & Juanes, R 2019, 'Comprehensive comparison of pore-scale models for multiphase flow in porous media', *Proceedings of the National Academy of Sciences of the United States of America*, vol. 116, no. 28, pp. 13799-13806. <https://doi.org/10.1073/pnas.1901619116>

**Digital Object Identifier (DOI):**

[10.1073/pnas.1901619116](https://doi.org/10.1073/pnas.1901619116)

**Link:**

[Link to publication record in Heriot-Watt Research Portal](#)

**Document Version:**

Peer reviewed version

**Published In:**

Proceedings of the National Academy of Sciences of the United States of America

**Publisher Rights Statement:**

Published under the PNAS license.

**General rights**

Copyright for the publications made accessible via Heriot-Watt Research Portal is retained by the author(s) and / or other copyright owners and it is a condition of accessing these publications that users recognise and abide by the legal requirements associated with these rights.

**Take down policy**

Heriot-Watt University has made every reasonable effort to ensure that the content in Heriot-Watt Research Portal complies with UK legislation. If you believe that the public display of this file breaches copyright please contact [open.access@hw.ac.uk](mailto:open.access@hw.ac.uk) providing details, and we will remove access to the work immediately and investigate your claim.

# Comprehensive comparison of pore-scale models for multiphase flow in porous media

Benzhong Zhao<sup>a</sup>, Christopher W. MacMinn<sup>b</sup>, Bauyrzhan K. Primkulov<sup>c</sup>, Yu Chen<sup>d</sup>, Albert J. Valocchi<sup>d</sup>, Jianlin Zhao<sup>e</sup>, Qinqun Kang<sup>f</sup>, Kelsey Bruning<sup>g</sup>, James E. McClure<sup>h</sup>, Cass T. Miller<sup>g</sup>, Abbas Fakhari<sup>i</sup>, Diogo Bolster<sup>i</sup>, Thomas Hiller<sup>j</sup>, Martin Brinkmann<sup>k</sup>, Luis Cueto-Felgueroso<sup>l</sup>, Daniel A. Cogswell<sup>m</sup>, Rahul Verma<sup>n</sup>, Maša Prodanović<sup>n</sup>, Julien Maes<sup>o</sup>, Sebastian Geiger<sup>o</sup>, Morten Vassvik<sup>p</sup>, Alex Hansen<sup>p</sup>, Enrico Segre<sup>q</sup>, Ran Holtzman<sup>r</sup>, Zhibing Yang<sup>s</sup>, Chao Yuan<sup>t</sup>, Bruno Chareyre<sup>t</sup>, and Ruben Juanes<sup>c,1</sup>

<sup>a</sup>McMaster University, Hamilton, ON, Canada; <sup>b</sup>University of Oxford, Oxford, UK; <sup>c</sup>Massachusetts Institute of Technology, Cambridge, MA, USA; <sup>d</sup>University of Illinois at Urbana-Champaign, Urbana, IL, USA; <sup>e</sup>Swiss Federal Institute of Technology in Zürich, Zürich, Switzerland; <sup>f</sup>Los Alamos National Laboratory, Los Alamos, NM, USA;

<sup>g</sup>University of North Carolina at Chapel Hill, Chapel Hill, NC, USA; <sup>h</sup>Virginia Polytechnic Institute & State University, Blacksburg, VA, USA; <sup>i</sup>University of Notre Dame, Notre Dame, IN, USA; <sup>j</sup>Leibniz Institute for Applied Geophysics, Hannover, Germany; <sup>k</sup>Saarland University, Saarbrücken, Germany; <sup>l</sup>Universidad Politécnica de Madrid, Madrid, Spain; <sup>m</sup>Aramco Services Company: Aramco Research Center-Boston, Cambridge, MA, USA; <sup>n</sup>University of Texas at Austin, Austin, TX, USA; <sup>o</sup>Heriot-Watt University, Edinburgh, UK; <sup>p</sup>Norwegian University of Science and Technology, Trondheim, Norway; <sup>q</sup>Weizmann Institute of Science, Rehovot, Israel; <sup>r</sup>The Hebrew University of Jerusalem, Rehovot, Israel; <sup>s</sup>Coventry University, Coventry, UK; <sup>t</sup>Wuhan University, Wuhan, China; <sup>1</sup>Grenoble Institute of Technology, Grenoble, France

**Multiphase flows in porous media are important in many natural and industrial processes. Pore-scale models for multiphase flows have seen rapid development in recent years, and are becoming increasingly useful as predictive tools in both academic and industrial applications. However, quantitative comparisons between different pore-scale models, and between these models and experimental data, are lacking. Here, we perform an objective comparison of a variety of state-of-the-art pore-scale models, including lattice Boltzmann, stochastic rotation dynamics, volume-of-fluid, level-set, phase-field, and pore-network models. As the basis for this comparison, we use a dataset from recent microfluidic experiments with precisely controlled pore geometry and wettability conditions, which offers an unprecedented benchmarking opportunity. We compare the results of the 14 participating teams both qualitatively and quantitatively using several standard metrics, such as fractal dimension, finger width, and displacement efficiency. We find that no single method excels across all conditions, and that thin films and corner flow present substantial modelling and computational challenges.**

porous media | capillarity | wettability | pattern formation | simulation

**M**ultiphase flows in porous media are central to a wide range of natural and industrial processes, including geologic CO<sub>2</sub> sequestration, enhanced oil recovery, and water infiltration into soil. Predictive modelling of these processes requires a clear understanding of the pore-scale mechanisms of fluid-fluid displacement. These pore-scale processes can be simulated using a variety of different approaches, including lattice/particle-based methods such as the lattice Boltzmann method, upscaled continuum methods such as phase-field models, and topological methods such as pore-network models (1). All of these models must confront a variety of fundamental challenges related to resolving the combined effects of capillarity, wetting, and viscous instability within a complex geometry, including thin films, moving contact lines, and the pinch-off and merging of interfaces. These mechanisms combine to produce macroscopic displacement patterns that are strongly dependent on the relative affinity of the solid for the different fluids (*i.e.*, wettability), the importance of viscous forces relative to capillary forces (*i.e.*, capillary number), and the pore geometry. As a result, pore-scale modelling of multiphase flow in porous media, even for relatively simple pore geometries, remains an open challenge and a very active area of research.

Historically, comparisons between pore-scale models and experimental data have been hampered by limitations on both fronts. The vast majority of existing experimental observations have been limited to macroscopic features and a narrow range of wettability conditions (strong drainage), and do not include a precise description of the associated pore geometry. In addition, most pore-scale models are very computationally expensive; only recently have these methods been able to simulate flow through a sufficiently large number of pores to reproduce macroscopic observables thanks to advances in both modelling methods and computing power. At the same time, modern experimental techniques now allow for high-resolution experimental observations and detailed characterization of pore geometry (1). One recent dataset, in particular, provides high-resolution observations across a wide range of wettabilities and capillary numbers in a well-defined and relatively simple pore geometry (2). These observations offer an unprecedented benchmarking opportunity for pore-scale models. The goal of this benchmark is to compare a wide variety of state-of-the-art pore-scale modelling approaches with experimental observations in terms of both pore-scale mechanisms

## Significance Statement

The simultaneous flow of multiple fluid phases through a porous solid occurs in many natural and industrial processes. *Microscale* physical mechanisms such as the relative affinity of the solid for the fluids (*i.e.*, wettability), capillarity, and viscosity combine with pore geometry to produce a wide variety of *macroscopic* flow patterns. Pore-scale modeling is an essential tool to connect microscale mechanisms with macroscopic patterns, but quantitative comparisons between different models, and with experimental data, are lacking. Here, we perform an unprecedented comparison of state-of-the-art models from 14 leading groups with a recent experimental dataset. The results underscore the challenges of simulating multiphase flows through porous media, highlighting specific areas for further effort in what is already a flourishing field of research.

Please provide details of author contributions here.

The authors declare no conflict of interest.

<sup>1</sup>To whom correspondence should be addressed. E-mail: juanes@mit.edu



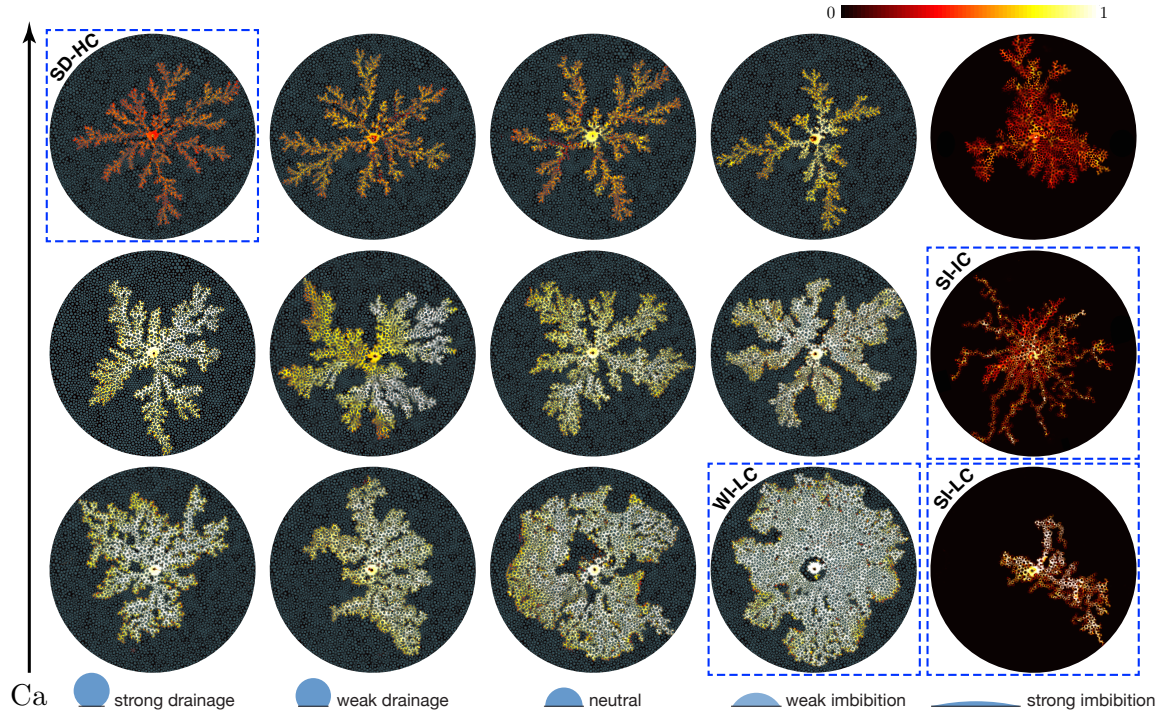


**Fig. 1.** Experimental phase diagram showing the displacement pattern at breakthrough for different wettability conditions (left to right:  $\theta = 150^\circ$ ,  $120^\circ$ ,  $90^\circ$ ,  $60^\circ$ ,  $7^\circ$ ) and capillary numbers (bottom to top:  $Ca = 0.029$ ,  $0.29$ ,  $2.9$ ). The colormap shows the gap-averaged saturation of the invading fluid. The four “priority cases” for the benchmark study are outlined in dashed blue: Strong drainage at high  $Ca$  (SD-HC), weak imbibition at low  $Ca$  (WI-LC), strong imbibition at intermediate  $Ca$  (SI-IC), and strong imbibition at low  $Ca$  (SI-LC). *Adapted from (2).*

and macroscopic displacement patterns.

## Results

**Dataset.** The benchmark study is based on the experiments of Zhao *et al.* (2) (Fig. 1). In the experiments, water was injected ( $\eta_{\text{water}} = 0.99 \text{ mPa} \cdot \text{s}$ ) into a viscous silicone oil ( $\eta_{\text{oil}} = 340 \text{ mPa} \cdot \text{s}$ ) in quasi-2D microfluidic flow cells patterned with vertical posts. This is a strongly viscously unstable displacement with viscosity ratio  $\mathcal{M} = \eta_{\text{oil}}/\eta_{\text{water}} \approx 340$ . The large unfavorable viscosity ratio of the experimental dataset was motivated by several considerations: it allows for direct comparison with previous wettability-related experimental studies (3, 4), it helps to highlight the impact of wettability on viscous instabilities, and it is directly relevant to applications like waterflooding of heavy crude oil (5).

The importance of viscous forces relative to capillary forces in the experiments was characterized using the classical capillary number  $Ca = \eta_{\text{oil}} v_{\text{inj}}/\gamma$ , where  $\gamma = 13 \pm 2 \text{ mN/m}$  is the interfacial tension between the fluids and  $v_{\text{inj}} = Q/(bd)$  is the characteristic injection velocity as constrained by the gap thickness  $b = 100 \text{ } \mu\text{m}$  and the median pore-throat size  $d = 300 \text{ } \mu\text{m}$ . The experiments were conducted at three distinct values of  $Ca$  spanning two orders of magnitude:  $Ca = 0.029$  (“low  $Ca$ ”),  $0.29$  (“intermediate  $Ca$ ”), and  $2.9$  (“high  $Ca$ ”).\* Note that these values of  $Ca$  provide a nominal macroscopic characterisation of the flow, but the actual strength of viscous to capillary forces varies locally due pore-scale heterogeneity, preferential pathways, and the radial flow geometry. Note also that the lowest value of  $Ca$  considered here is still moderate relative to

a truly quasi-static displacement. The wettability of the flow cell was characterized using the static advancing contact angle  $\theta$  of water immersed in silicone oil. The experiments were conducted at five distinct values of  $\theta$  spanning the full range of wettability conditions:  $\theta = 150^\circ$  (“strong drainage”),  $120^\circ$  (“weak drainage”),  $90^\circ$  (“neutral”),  $60^\circ$  (“weak imbibition”), and  $7^\circ$  (“strong imbibition”). The participating teams were given the exact geometry of the post pattern and, for each experimental condition, a series of data files describing the time evolution of the gap-averaged water saturation  $S$  at high spatial resolution. To allow for qualitative and quantitative comparisons between methods without imposing an excessive computational burden on participants, we identified four “priority cases” that best represent the diversity of patterns and physical mechanisms that emerge from fluid-fluid displacement under different  $Ca$  and wettability conditions:

1. Strong drainage at high  $Ca$  (SD-HC): Canonical viscous fingering pattern with incomplete pore-scale displacement due to formation of trailing films of the defending fluid.
2. Weak imbibition at low  $Ca$  (WI-LC): Compact displacement pattern due to cooperative pore filling.
3. Strong imbibition at intermediate  $Ca$  (SI-IC): Thin-film flow of the invading fluid along the top and bottom walls, accompanied by a ramified fingering pattern formed by corner flow.
4. Strong imbibition at low  $Ca$  (SI-LC): Corner-flow-driven “chaining” of posts.

**Participating teams and methods.** A total of 14 teams contributed modelling results to the benchmark study (Table 1).

\*Note that the  $Ca$  values reported in (2) are incorrect—They are too small by one order of magnitude.

Label	Authors	Method	Dim.	Comp. Dom.	Res.	$\mathcal{M}$	Remarks	Refs.
<b>LB1</b>	Y. Chen A. Valocchi	Lattice Boltzmann	3	50%, 80%	14.3	5, 40, 100	Artificial precursor film in strong imbibition.	(6, 7)
<b>LB2</b>	J. Zhao Q. Kang	Lattice Boltzmann	2	100%	20.2	340	Perturbation & recoloring operators generate interfacial tension & phase segregation, respectively.	(8, 9)
<b>LB3</b>	K. Bruning J. McClure C. Miller	Lattice Boltzmann	3	40%	13	100	Increased domain thickness to 448 $\mu\text{m}$ to better resolve film formation in the gap.	(10, 11)
<b>LB4</b>	A. Fakhari D. Bolster	Lattice Boltzmann	2	100%	$\sim 100$	340	LB equation based on the conservative phase-field method.	(12, 13)
<b>SR1</b>	T. Hiller M. Brinkmann	Stochastic rotation dynamics	3	60%	$\sim 300$	1–5	Limited resolution in the gap, leading to unrepresentative saturation.	(14, 15)
<b>PF1</b>	L. Cueto-Felgueroso	Phase field	2	100%	$\sim 30$	340	Diffuse interface model that captures 3D physics.	(16, 17)
<b>PF2</b>	D. Cogswell	Phase field	2	100%	$\sim 50$	340	Variational boundary condition sets the contact angle.	(18)
<b>LS1</b>	R. Verma M. Prodanovic	Level set	2	100%	24.9	n.a.	Quasi-static; simulates trapped fluid via immobile "masks".	(19–22)
<b>VF1</b>	J. Maes	Volume-of-fluid	2	100%, 60%	$\sim 80$	340	Implemented in OpenFOAM as an internal VOF solver ( <i>interFoam</i> ).	(23, 24)
<b>PN1</b>	S. Geiger M. Vassvik	Pore network	2	100%	n.a.	340	Single pressure, dynamic model; ignores the out-of-plane curvature.	(25, 26)
<b>PN2</b>	A. Hansen E. Segre	Pore network	2	100%	n.a.	340	Single pressure, dynamic model; ignores the out-of-plane curvature.	(27, 28)
<b>PN3</b>	R. Holtzman B. Primkulov B. Zhao C. W. MacMinn	Pore network	2	100%	n.a.	340	Single pressure, dynamic model; includes the out-of-plane curvature; quasi-static version of the model captures corner flow.	(29, 30)
<b>PN4</b>	R. Juanes Z. Yang	Pore network	2	100%	n.a.	340	Single pressure, dynamic model; includes the out-of-plane curvature.	(31)
<b>PN5</b>	C. Yuan B. Chareyre	Pore network	2	100%	n.a.	n.a.	Quasi-static model for strong drainage; includes the out-of-plane curvature.	(32, 33)

**Table 1.** Summary of contributions. See *SI Appendix* Note 3–5 for further details on methods. Dim.: Dimensionality. Comp. Dom.: Radius of computational domain as a percentage of the radius of the experimental domain. Res.: Resolution of the computational domain in  $\mu\text{m}$  per grid block/lattice.

Together, they applied many different pore-scale modelling methods (Table 1 and *SI Appendix* Note 1). The methods can be categorized into three major classes: lattice/particle-based models, continuum models, and pore-network models. Lattice/particle-based models simulate the motion and interaction of a large number of microscopic particles that collectively give rise to macroscopic behavior satisfying the relevant continuum equations (e.g., Navier-Stokes). The fluid-fluid interface is captured implicitly as the boundary between the multi-colored particles that represent the different fluid phases. These models include the lattice Boltzmann (LB) methods (34) and stochastic rotation dynamics (SR) models (35). Continuum models solve macroscopic equations for fluid flow while tracking the interface implicitly via the evolution of an indicator variable. These models include volume-of-fluid (VF) methods (36), level-set (LS) methods (37), and phase-field (PF) models (38). Pore-network (PN) models simulate fluid flow through an idealized network of pores connected by throats (39). The macroscopic interface is represented explicitly as the boundary between invaded and non-invaded pores. It speaks to the physical complexity of this problem that only one of the contributions (VF1) attempted direct simulation of the Navier-Stokes (or Stokes) equations with evolving fluid-fluid interfaces. Note also that only LB1, LB3, and SR1 conducted truly 3D simulations.

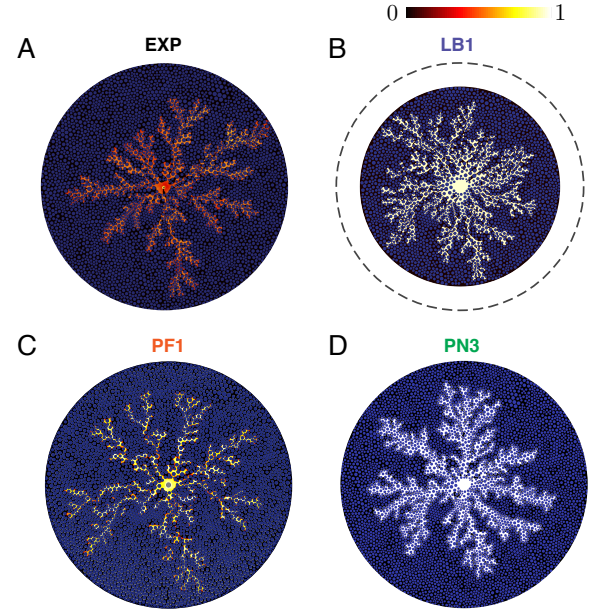
**Qualitative performance measures.** The interplay between wettability and Ca generates a wide spectrum of 2D displacement patterns that range from ramified fingers to compact fronts (Fig. 1). Additional 3D information is provided by the local gap-averaged saturation of the invading fluid (Fig. 1). The displacement pattern and saturation distribution at the end of the simulation, when the invading fluid reaches the outer edge of the computational domain, serve as a good basis for qualitative and quantitative comparisons (e.g., Fig. 3 & *SI Appendix*).

**Quantitative performance measures.** For quantitative comparison, we calculate four performance measures from the displacement pattern at the end of each simulation, when the invading fluid reaches the outer edge of the domain:

1. Fractal dimension  $D_f$ , as calculated via the box-counting method. This is a classical measure of the degree to which a pattern fills space in 2D (40).
2. Average dimensionless finger width  $W_f$ , as measured at half the radius of the computational domain and scaled by the median post diameter. Note that this measure is very sensitive to domain size for compact displacements, and that not all groups used the same domain size.
3. Gap-averaged saturation  $S$  of the invading fluid, as represented by its median value as well as the first and third quartiles. Note that many methods ignore films and therefore assume  $S = 1$  in invaded regions.
4. Displacement efficiency  $E_d$ , which is the fraction of the defending fluid that has been displaced from the domain.

Details on how we calculated the quantitative performance measures can be found in *SI Appendix* Note 2.

**Submission of simulation results.** While some teams submitted results for many of the conditions in the experimental phase



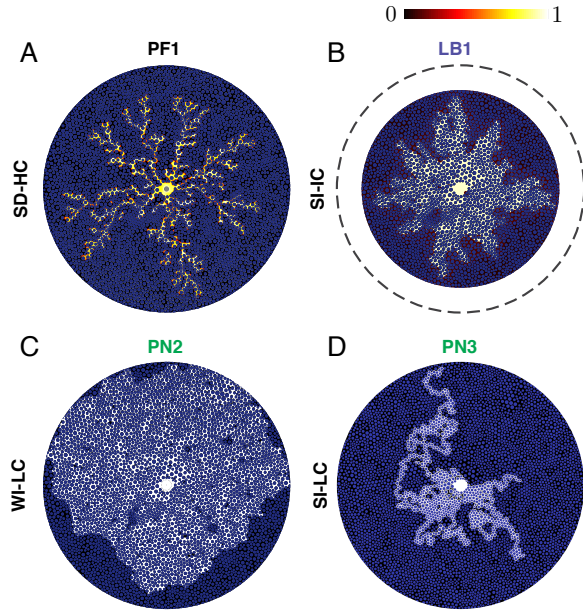
**Fig. 2.** Comparison between (A) the experimental displacement pattern and (B–D) selected simulated displacement patterns for the case of strong drainage at high Ca (SD-HC). The simulations capture the slender, ramified fingering patterns of SD-HC well, though they are produced by three distinctly different classes of modeling methods. The three methods differ most strongly in how well they reproduce the residual wetting films, as illustrated by the colormap.

diagram (Fig. 1), most teams only contributed results for a relevant subset of the priority cases (Table 1, *SI Appendix*). For example, some methods were developed for quasi-static displacement (*i.e.*, small Ca; LS1, PN5), and therefore could not be applied to intermediate or high Ca conditions. Other methods were developed for drainage only (PN4, PN5), and therefore could not be applied to imbibition scenarios. Additionally, some teams simulated a subset of the experimental domain (*i.e.* truncated at a smaller outer radius; LB1, LB3, SR1, VF1) due to computational constraints.

**Performance of the methods. SD-HC:** The experimental displacement pattern for SD-HC displays classical viscous fingering, known for the slender, ramified fingers mimicked by diffusion-limited aggregation (Fig. 1) (41, 42). Remarkably, all three classes of methods are able to capture these patterns (Fig. S1). Quantitative analysis of the simulated patterns reveals that while most methods reproduce  $W_f$  to within a factor of 60%, most methods overpredict  $D_f$ , and all methods overpredict  $E_d$ , often by several-fold (Fig. 4A). The latter discrepancy is a consequence of incomplete pore-scale displacement due to the well-known formation of thin trailing films of the defending fluid at high Ca (43, 44). Most methods ignore these films, and those that capture them tend to underpredict their thickness, which corresponds to over-predicting  $S$  (Fig. 4A). The PF methods appear to do a reasonable job of capturing this incomplete displacement without simulating the full 3D problem. Note that LB1, LB3, SR1, and VF1 simulate a subset of the full domain, and that LB1, LB3, and SR1 simulate at a reduced  $\mathcal{M}$ . Displacement at high Ca is very sensitive to viscosity ratio, and the predictions of the latter methods are affected accordingly.

**WI-LC:** The experimental displacement pattern for WI-





**Fig. 3.** Selection of simulated displacement patterns for the priority cases. (A) Strong drainage at high Ca (SD-HC) as simulated by a phase-field model. (B) Strong imbibition at intermediate Ca (SI-IC) as simulated by a lattice Boltzmann model at a reduced viscosity ratio ( $\mathcal{M} = 40$ ). (C) Weak imbibition at low Ca (WI-LC) as simulated by a pore-network model. (D) Strong imbibition at low Ca (SI-LC) as simulated by a pore-network model.

LC shows compact displacement as a result of cooperative pore filling (27, 45). Qualitatively, all three classes of methods are again able to capture these patterns (Fig. S2). Most methods capture  $D_f$  to within a few percent, suggesting that the methods reproduce the 2D features of the pattern (Fig. 4B). This case does not feature thin films, so  $S$  is nearly 1; as a result, those methods that capture  $D_f$  well also capture  $E_d$ . Note that LB1, SR1, and VF1 simulate a subset of the full domain, and LB1 and SR1 simulate at a reduced  $\mathcal{M}$ . Displacement at low Ca is not very sensitive to viscosity ratio, so the latter two methods still perform well in this scenario.

**SI-IC:** The experimental displacement pattern for SI-IC shows a highly ramified, yet roughly axisymmetric fingering pattern, the backbone of which is formed by the successive “chaining” of posts by preferential flow along the post-wall corners (2). The resulting pattern has low values of  $S$  because the strongly wetting invading fluid propagates primarily by corner flow and in thin films along the top and bottom walls, bypassing pore bodies (2, 46, 47). Qualitatively, none of the methods reproduce the ramified backbone of linked posts (Fig. S3). Most methods fail to capture the emergence of corner flow, typically overestimating  $W_f$  and greatly overestimating  $E_d$  (Fig. 4C). Fully 3D methods should be able to capture corner flow and film flow, and images from the 3D simulations (LB1, LB3, SR1) suggest that they do, at least to some extent (Fig. 5). However, because of the high computational demands, all three of these methods simulate subsets of the full domain at greatly reduced  $\mathcal{M}$ ; the latter suppresses the strong preferential flow through thin films that should occur for large  $\mathcal{M}$ . Quasi-3D (gap-averaged) phase-field methods (PF1, PF2) can capture film flow through their upscaled representation of the affinity of the invading fluid for both the walls and the posts, but cannot capture corner

flow without an explicit sub-model for the presence of corners. Pore-network models would require explicit sub-models for both film flow and corner flow.

**SI-LC:** The experimental displacement pattern for SI-LC is completely controlled by nearly quasi-static invasion through corner flow. Corner films link groups of posts via bursts, and then surrounded pores fill slowly and almost completely. Unlike SI-IC, these patterns have a relatively large value of  $S$  and no axial symmetry or well-defined fingers or branches. Relatively few participants attempted this case because it involves both low Ca (computationally demanding for 3D methods) and corner flow (absent from most methods). Qualitatively, the simulation results are quite variable (Fig. S4). PN3 captures post-chaining via corner flow with a dedicated sub-model for corner flow, but does not capture the subsequent filling-in (Fig 3); PF1 captures the rough shape, but without clear post-chains. Quantitatively, all methods over-predict  $D_f$ , but all methods are relatively close to the experimental value (Fig. 4D). All methods except for PF1 also over-predict  $W_f$  by a factor of 2 or more. Only PF1 and PF2 are able to make quantitative predictions of  $S$  (SR1, PN2, and PN3 assume  $S = 1$ ); PF1 reproduces the experimental value of  $S$  very closely, whereas PF2 significantly over-predicts  $S$ . PF1 and PN3 both capture  $E_d$  relatively well; PF1 is arguably the best match overall.

**Thin films and corner flow.** The complex nature of interfacial flows in the presence of solid surfaces lends an inherently 3D nature to fluid-fluid displacement processes, even in quasi-1D geometries such as capillary tubes (48) and quasi-2D geometries such as Hele-Shaw cells (46). In a patterned micromodel, these 3D effects include the propagation of thin films along the top and bottom walls and the surfaces of the posts, and in the corners where the walls and posts meet (2, 47). While both fully 3D methods (LB1, LB3) and quasi-3D (gap-averaged) methods (PF1, PF2) predict the formation of trailing films in SD-HC, only fully 3D methods (LB1, LB3) capture films in SI-IC. The color-gradient wetting model used in LB1 leads to an artificial film ( $\sim 14 \mu\text{m}$ ) that slowly permeates the entire simulation domain. This film accumulates on the posts to form corner films and pendular rings that resemble those observed in the experiments (Fig. 5B). However, this film also uniformly coats the top and bottom walls, and the resulting mass transport appears to suppress the strong preferential flows observed in the experiment. LB3 uses a similar wetting model, and should therefore have the same feature (Fig. 5C). Both of these methods are very computationally demanding due to the very large number of particles needed to resolve a 3D flow. For a given scenario, the computational cost also scales with the number of timesteps and the timestep size. The timestep size is constrained by  $\mathcal{M}$  for numerical stability, whereas the number of timesteps to breakthrough scales with the domain size. As a result, LB1 and LB3 simulate a subset of the full domain, and at a reduced  $\mathcal{M}$ .

## DISCUSSION

The goal of this benchmark study was to assess the degree to which different state-of-the-art modeling strategies could reproduce the correct macroscopic features (and some pore-scale features) of fluid-fluid displacement in a porous medium under different wetting conditions. These pore-scale models have

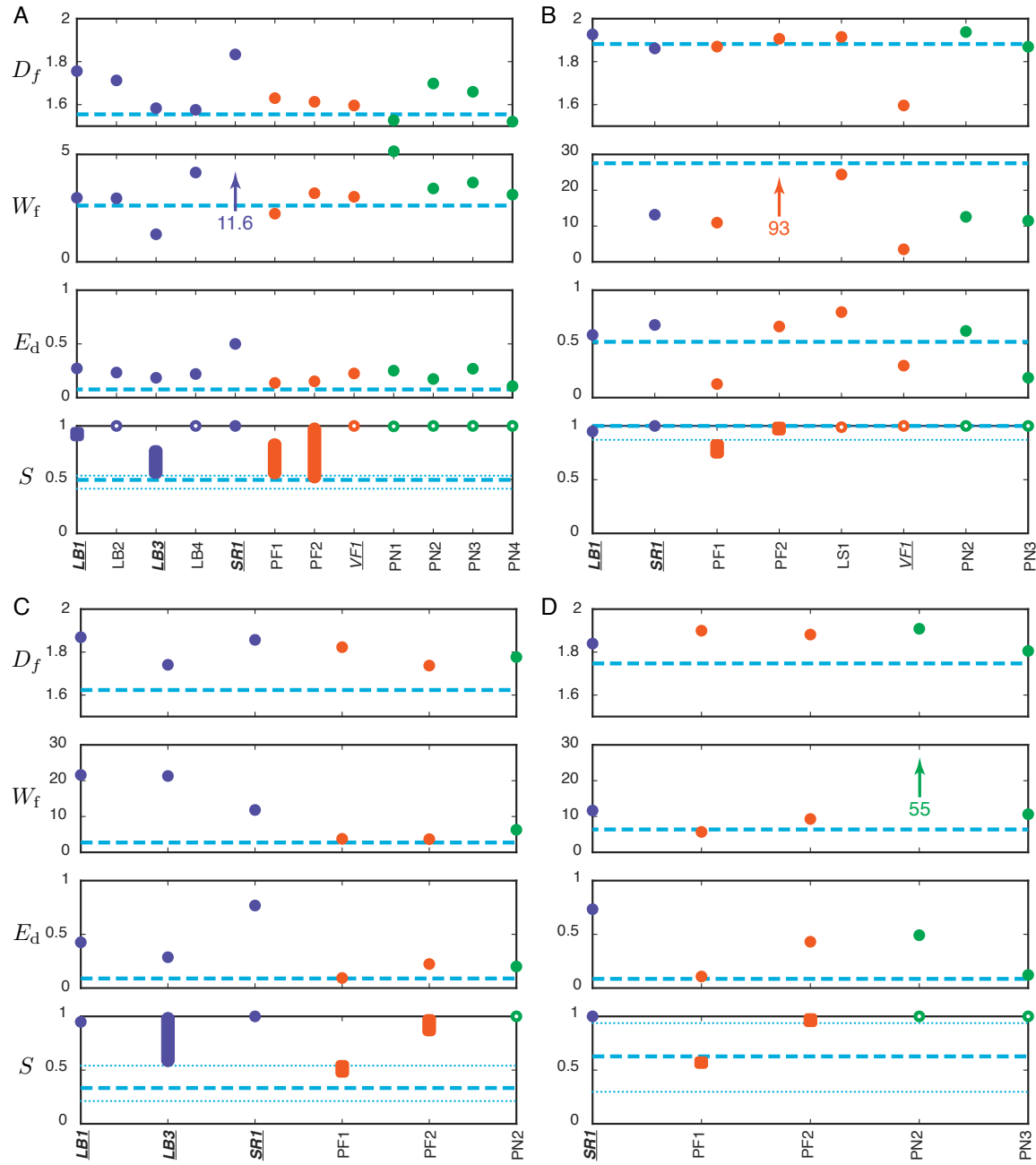


**Fig. 4.** Quantitative performance results for (A) SD-HC, (B) WI-LC, (C) SI-IC, and (D) SI-LC. First row: Fractal dimension  $D_f$ . Second row: Average dimensionless finger width  $W_f$ . Third row: Displacement efficiency  $E_d$ . Fourth row: Gap-averaged saturation  $S$  of the invading fluid in invaded regions, with symbols spanning the range from first quartile to third quartile. In the latter, open circles indicate methods that neglect films and therefore assume  $S = 1$  in invaded regions. In all cases, we also plot the corresponding experimental measurement (dashed blue line); for  $S$ , we show the first and third quartiles (dotted blue lines) in addition to the median value. *Italic labels* on the horizontal axis denote contributions that simulate a subset of the experimental domain, while **bold labels** denote contributions that simulate at a reduced  $\mathcal{M}$  relative to the experiments.

become widely-used tools in extracting macroscopic properties of geologic porous media (*e.g.*, relative permeability) (49–52), and in designing synthetic porous materials with desirable transport properties in electrochemical devices (53, 54). In all these cases, the accuracy of the model output hinges upon its ability to correctly account for the impact of wettability at different capillary numbers.

Most methods were able to capture viscous instability and fingering at high flow rates (IC and HC), and most were also able to capture the more subtle broadening of features in WI

where the low contact angle enables cooperative pore filling. In contrast, few methods were able to capture the thin trailing films that form for SD-HC, the thin leading films that occur for SI-IC, and the corner films that dominate SI-LC, all of which are inherently 3D.

For 2D models, films present a modelling challenge. Gap-averaged PF models were able to capture trailing films in SD-HC, although leading films in SI-IC and corner flow in SI-LC remain elusive. Other 2D models were unable to capture films to any noteworthy extent. PN3 was the only model to explicitly



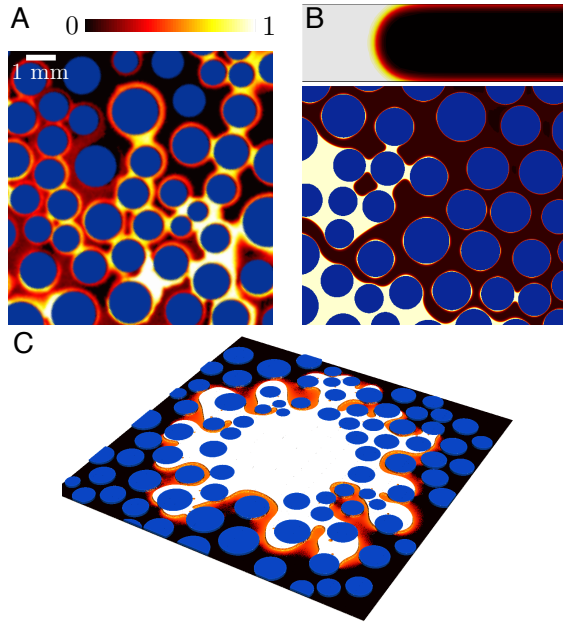


**Fig. 5.** (A) Experimental snapshot of SI-IC at the pore scale, which is characterized by the co-existence of thin films and corner flow. (B) Simulation results of LB1 for SI-IC ( $\mathcal{M} = 40$ ). Top: Cross-sectional view showing the leading thin films along the top and bottom walls. Bottom: Plan view showing the co-existence of thin films and corner flow, as well as pendular rings that link neighboring posts. (C) Isometric projection of the 3D simulation results of LB3 for SI-IC ( $\mathcal{M} = 100$ ), showing the propagation of thin films ahead of the main invasion front.

account for corner flow, and was reasonably successful in doing so for quasi-static displacement. However, extending such a model to include viscous effects and residual films is nontrivial because many of the underlying physical phenomena, such as flow through corner networks, film bridging from post to post, and post-chaining avalanches, are poorly understood.

For 3D models, films present a serious computational challenge. Resolving films is nontrivial due to the large aspect ratio of the problem—the flow cell has a radius of 100 mm, the gap thickness is 100  $\mu\text{m}$ , and the film thickness ranges from tens of microns to a few microns or less. LB1, LB2, and LB3 addressed this challenge most directly, running 3D simulations with  $\sim 160$  million,  $\sim 160$  million, and  $\sim 300$  million lattice sites, respectively. Even after reducing the viscosity ratio and truncating the domain in order to relax time-step restrictions, these simulations required world-class computational resources. Despite this substantial effort, these simulations could only achieve a spatial resolution of 10–20  $\mu\text{m}$ , which is barely small enough to allow for films and certainly not small enough to resolve them. All three groups agree that this problem pushes the limits of what is currently possible. More importantly, these simulations showed both qualitatively and quantitatively that failure to resolve films at the small-scale can have important consequences for the *macroscopic flow pattern*.

It is well-known that pre-existing wetting films are common in subsurface applications such as enhanced oil recovery, and that their presence has a significant impact on the macroscopic transport properties such as relative permeability (55, 56). These pre-existing films would be an active, evolving component of the displacement as they swell, disconnect, reconnect, and pinch-off—particularly in partial wetting conditions. Re-

solving them (and the flow within them) would be an essential and challenging part of the problem.

This benchmark targets the “many-pore” scale (hundreds to thousands of pores), as this is a scale large enough to manifest the collective dynamics characteristic of fluid–fluid displacements in porous media (viscous fingering, capillary fingering, avalanches, etc.), and small enough that computational models are routinely used to make predictions. Thus, it is natural to ask whether those predictions are accurate. There is, however, an underlying scale at which “single-pore” fluid-mechanics details emerge (such as menisci deformation and merging, contact-line pinning and motion, contact-angle hysteresis, post wetting dynamics, etc). The inclusion of these effects will further increase the computational complexity of the problem, which makes it impractical at the scale of hundreds to thousands of pores considered in the current study, and comparison of different methods at this single-pore scale would require an altogether different type of benchmark study in a simpler geometry (e.g., Verma *et al.*, 2018 (21)). Furthermore, real rocks such as carbonates also have a wider pore size distribution than the one from our micromodel (57), a feature that would likely have an effect on the correlation between pore occupancy and pore size that is absent from our experimental benchmark.

A key contribution of this benchmark is to demonstrate the capabilities and limitations of three major classes of pore-scale models (*i.e.*, lattice/particle-based models, continuum models, and pore-network models) in predicting the macroscopic features of unstable two-phase flows in the presence of solid surfaces. We find that all three classes of models are capable of predicting the transition from strong drainage to weak imbibition. Specifically, pore-network models offer superior computational efficiency, but they lack the ability to resolve gap-averaged saturations that the more computationally intensive lattice/particle-based models and continuum models offer. Only 3D lattice/particle-based models could simulate leading films and corner flow in strong imbibition, but their spatial and temporal resolutions are severely limited by the prohibitive computational demand. Our results highlight the need for further effort along multiple complementary avenues in what is already a very active area of research.

## Materials and Methods

The simulated displacement patterns for all priority cases are presented in *SI Appendix*, Figs. S1–S4. Details on how we calculated the quantitative performance measures of the priority cases can be found in *SI Appendix* Note 2. Descriptions of all the models, including their derivation and numerical implementation, are included in *SI Appendix* Note 3–5.

**ACKNOWLEDGMENTS.** A.V. and Y.C.: Center for Geologic Storage of CO<sub>2</sub>, an Energy Frontier Research Center funded by the US Department of Energy (DOE), Office of Science, Basic Energy Sciences (Award DE-SC0012504) and TACC Stampede 2 system (Allocation ID: EAR160028) provided by Extreme Science and Engineering Discovery Environment (XSEDE); Q.K: Los Alamos National Lab’s Laboratory Directed Research & Development Program and Institutional Computing Program; K.B., J.E.M., and C.T.M.: US Army Research Office (Grant No. W911NF1410287), US National Science Foundation (Grant No. 1619767), the US DOE INCITE program (computer time), and the Oak Ridge Leadership Computing Facility (computing resources), which is a US DOE Office of Science User Facility (Contract No. DE-AC05-00OR22725);

395 A.F. and D.B.: US National Science Foundation (NSF) (Grant  
396 No. CBET-1705770); R.V. and M.P.: US NSF EAR CAREER  
397 (Grant No. 1255622); J.M. and S.G.: UK Engineering and Physical  
398 Sciences Research Council (Grant EP/P031307/1) and funding from  
399 Energi Simulation; M.V. and A.H.: Centers of Excellence funding  
400 scheme, Research Council of Norway (Project No. 262644); R.H.:  
401 Israeli Science Foundation (Grant No. ISF-867/13) Z.Y.: National  
402 Natural Science Foundation of China (Grant No. 41877203); B.P.  
403 and R.J.: US Department of Energy (Grant No. DE-SC0018357).

404 1. Blunt MJ, et al. (2013) Pore-scale imaging and modelling. *Adv. Water Resour.* 51:197–216.  
405 2. Zhao B, MacMinn CW, Juanes R (2016) Wettability control on multiphase flow in patterned  
406 microfluidics. *Proc. Natl. Acad. Sci. USA* 113(37):10251–10256.  
407 3. Stokes JP, et al. (1986) Interfacial stability of immiscible displacement in a porous medium.  
408 *Phys. Rev. Lett.* 57:1718–1721.  
409 4. Trojer M, Szulcowski ML, Juanes R (2015) Stabilizing fluid-fluid displacements in porous  
410 media through wettability alteration. *Phys. Rev. Applied* 3:054008.  
411 5. Al-Besharah JM, Salman OA, Akashah SA (1987) Viscosity of crude oil blends. *Ind. Eng.*  
412 *Chem. Res.* 26:2445–2449.  
413 6. Chen Y, Li Y, Valocchi AJ, Christensen KT (2018) Lattice Boltzmann simulations of liquid  
414 CO<sub>2</sub> displacing water in a 2D heterogeneous micromodel at reservoir pressure conditions. *J.*  
415 *Contam. Hydrol.* 212(14–27).  
416 7. Zhao J, et al. (2016) Simulation of microscale gas flow in heterogeneous porous media based  
417 on the lattice Boltzmann method. *J. Appl. Phys.* 120:084306.  
418 8. Liu H, Valocchi AJ, Kang Q (2012) Three-dimensional lattice Boltzmann model for immiscible  
419 two-phase flow simulations. *Phys. Rev. E* 85(4):046309.  
420 9. Liu H, Valocchi AJ, Werth C, Kang Q, Oostrom M (2014) Pore-scale simulation of liquid  
421 CO<sub>2</sub> displacement of water using a two-phase lattice Boltzmann model. *Adv. Water Resour.*  
422 73:144–158.  
423 10. McClure JE, Prins JF, Miller CT (2014) A novel heterogeneous algorithm to simulate mul-  
424 tiphase flow in porous media on multicore CPU-GUP systems. *Comput. Phys. Commun.*  
425 185:1865–1874.  
426 11. McClure JE, Berrill MA, Gray WG, Miller CT (2016) Tracking interface and common curve  
427 dynamics for two-fluid-phase flow in porous media. *J. Fluid Mech.* 796:211–232.  
428 12. Fakhari A, Bolster D (2017) Diffuse interface modeling of three-phase contact line dynamics  
429 on curved boundaries: A lattice Boltzmann model for large density and viscosity ratios. *J.*  
430 *Comput. Phys.* 334:620–638.  
431 13. Fakhari A, Li Y, Bolster D, Christensen KT (2018) A phase-field lattice Boltzmann model for  
432 simulating multiphase flows in porous media: Application and comparison to experiments of  
433 CO<sub>2</sub> sequestration at pore scale. *Adv. Water Resour.* 114(119–134).  
434 14. Hiller T, Lama MSDL, Brinkmann M (2016) Stochastic rotation dynamics of wetting multi-  
435 phase flows. *J. Comput. Phys.* 315:554–576.  
436 15. Jung M, et al. (2016) Wettability controls slow immiscible displacement through local interface  
437 instabilities. *Phys. Rev. Fluids* 1:074202.  
438 16. Cueto-Felgueroso L, Juanes R (2014) A phase-field model of two-phase Hele-Shaw flow. *J.*  
439 *Fluid Mech.* 758:522–552.  
440 17. Cueto-Felgueroso L, Juanes R (2012) Macroscopic phase-field model of partial wetting: Bub-  
441 bles in a capillary tube. *Phys. Rev. Lett.* 108:144502.  
442 18. Cogswell DA, Szulcowski ML (2017) Simulation of incompressible two-phase flow in porous  
443 media with large timesteps. *J. Comput. Phys.* 345:856–865.  
444 19. Prodanović M, Bryant S (2006) A level set method for determining critical curvatures for  
445 drainage and imbibition. *J. Colloid Interface Sci.* 304(2):442–458.  
446 20. Jettsetuen E, Helland JO, Prodanović M (2013) A level set method for simulating capillary-  
447 controlled displacements at the pore scale with nonzero contact angles. *Water Resour. Res.*  
448 49(8):4645–4661.  
449 21. Verma R, Icardi M, Prodanović M (2018) Effect of wettability on two-phase quasi-static dis-  
450 placement: Validation of two pore scale modeling approaches. *J. Contam. Hydrol.* 212:115–  
451 133.  
452 22. Verma R (2018) PhD Thesis (The University of Texas at Austin, Austin, TX, USA).  
453 23. Pavuluri S, J. M, Doster F (2018) Spontaneous imbibition in a microchannel: analytical solu-  
454 tion and assessment of volume of fluid formulations. *Microfluidic Nanofluidic* (22:90).  
455 24. Maes J, Geiger S (2018) Direct pore-scale reactive transport modelling of dynamic wettability  
456 changes induced by surface complexation. *Adv. Water Resour* 111:6–19.  
457 25. Aker E, Mály KJ, Hansen A, Batrouni GG (1998) A two-dimensional network simulator for  
458 two-phase flow in porous media. *Transp. Porous Med.* 32:163–186.  
459 26. Knudsen HA, Aker E, Hansen A (2002) Bulk flow regimes and fractional flow in 2D porous  
460 media by numerical simulations. *Transp. Porous Med.* 47:99–121.  
461 27. Holtzman R, Segre E (2015) Wettability stabilizes fluid invasion into porous media via nonlo-  
462 cal, cooperative pore filling. *Phys. Rev. Lett.* 115:164501.  
463 28. Holtzman R (2016) Effects of pore-scale disorder on fluid displacement in partially-wettable  
464 porous media. *Sci. Rep.* 6(36221).  
465 29. Primkulov BK, et al. (2018) Quasi-static fluid-fluid displacement in porous media: Invasion-  
466 percolation through a wetting transition. *Phys. Rev. Fluids* 3:104001.  
467 30. Primkulov BK, et al. (year?) Signatures of fluid-fluid displacement in porous media: Wettabil-  
468 ity, invasion events, patterns, and pressures. *Submitted for publication*.  
469 31. Yang Z, Niemi A, Fagerlund F, Illangasekare T (2013) Two-phase flow in rough-walled frac-  
470 tures: Comparison of continuum and invasion-percolation models. *Water Resour. Res.*  
471 49:993–1002.  
472 32. Yuan C, Chareyre B, Darve F (2016) Pore-scale simulations of drainage in granular materials:  
473 finite size effects and the representative elementary volume. *Adv. Water Resour.* 97:109–124.  
474 33. Yuan C, Chareyre B (2017) A pore-scale method for hydromechanical coupling in deformable  
475 granular media. *Comput. Methods Appl. Mech. Eng.* 318:1066–1079.  
476 34. Chen S, Doolen GD (1998) Lattice Boltzmann method for fluid flows. *Annu. Rev. Fluid Mech.*  
30:329–364.  
35. Ihle T, Kroll DM (2001) Stochastic rotation dynamics: A Galilean-invariant mesoscopic model  
for fluid flow. *Phys. Rev. E* 63:020201.  
36. Hirt CW, Nichols BD (1981) Volume of fluid (VOF) method for the dynamics of free boundaries.  
*J. Comput. Phys.* 39:201–225.  
37. Sethian JA, Smereka P (2003) Level set methods for fluid interfaces. *Annu. Rev. Fluid Mech.*  
35:341–372.  
38. Badalassi VE, Cenicer HD, Banerjee S (2003) Computation of multiphase systems with  
phase field models. *J. Comput. Phys.* 190:371–397.  
39. Blunt MJ (2001) Flow in porous media — pore-network models and multiphase flow. *Curr.*  
*Opin. Colloid Interface Sci.* 6(197–207).  
40. Schroeder MR (2009) *Fractals, Chaos, Power Laws: Minutes from an Infinite Paradise.* (W.  
H. Freeman and Company), Dover edition.  
41. Paterson L (1984) Diffusion-limited aggregation and two-fluid displacements in porous media.  
*Phys. Rev. Lett.* 52(18):1621–1624.  
42. Måløy KJ, Feder J, Jossang T (1985) Viscous fingering fractals in porous media. *Phys. Rev.*  
*Lett.* 55:2688–2691.  
43. Taylor GI (1961) Deposition of a viscous fluid on the wall of a tube. *Journal of Fluid Mechanics*  
10(2):161–165.  
44. Bretherton FP (1961) The motion of long bubbles in tubes. *Journal of Fluid Mechanics*  
10(2):166–188.  
45. Cieplak M, Robbins MO (1990) Influence of contact angle on quasistatic fluid invasion of  
porous media. *Phys. Rev. B* 41(16):11508–11521.  
46. Levaché B, Bartolo D (2014) Revisiting the Saffman-Taylor experiment: Imbibition patterns  
and liquid-entrainment transitions. *Phys. Rev. Lett.* 113:044501.  
47. Odier C, Levaché B, Santanach-Carreras E, Bartolo D (2017) Forced imbibition in porous  
media: A fourfold scenario. *Phys. Rev. Lett.* 119:208005.  
48. Zhao B, Pahlavan AA, Cueto-Felgueroso L, Juanes R (2018) Forced wetting transition and  
bubble pinch-off in a capillary tube. *Phys. Rev. Lett.* 120:084501.  
49. Reeves PC, Celia MA (1996) A functional relationship between capillary pressure, satura-  
tion, and interfacial area as revealed by a pore-scale network model. *Water Resour. Res.*  
32(8):2345–2358.  
50. Rajaram H, Ferrand LA, Celia MA (1997) Prediction of relative permeabilities for unconsoli-  
dated soils using pore-scale network models. *Water Resour. Res.* 33(1):43–52.  
51. Valvatne PH, Blunt MJ (2004) Predictive pore-scale modeling of two-phase flow in mixed wet  
media. *Water Resour. Res.* 40:W07406.  
52. Hao L, Cheng P (2010) Pore-scale simulations on relative permeabilities of porous media by  
lattice Boltzmann method. *Int. J. Heat Mass Transf.* 53:1908–1913.  
53. Mukherjee PP, Kang Q, Wang CY (2011) Pore-scale modeling of two-phase transport in poly-  
mer electrolyte fuel cells – progress and perspective. *Energy Environ. Sci.* 4:346–369.  
54. Arbabi F, Montazeri H, Abouatallah R, Wang R, Bazylak A (2016) Three dimensional compu-  
tational fluid dynamics modelling of oxygen bubble transport in polymer electrolyte membrane  
electrolyzer porous transport layers. *J. Electrochem. Soc.* 163(11):F3062–F3069.  
55. Blunt M, King MJ, Scher H (1992) Simulation and theory of two-phase flow in porous media.  
*Phys. Rev. A* 46(12):7680–7699.  
56. Hui MH, Blunt M (2000) Effects of wettability on three-phase flow in porous media. *J. Phys.*  
*Chem. B* 104:3833–3845.  
57. Blunt MJ (2017) *Multiphase flow in permeable media: A pore-scale perspective.* (Cambridge  
University Press).